RESEARCH BRIEF

Analysis of Immune Signatures in Longitudinal Tumor Samples Yields Insight into Biomarkers of Response and Mechanisms of Resistance to Immune Checkpoint Blockade

Pei-Ling Chen[1,2], Whijae Roh[1], Alexandre Reuben[3], Zachary A. Cooper[1,3], Christine N. Spencer[1], Peter A. Prieto[3], John P. Miller[1], Roland L. Bassett[4], Vancheswaran Gopalakrishnan[3], Khalida Wani[5], Mariana Petaccia De Macedo[5], Jacob L. Austin-Breneman[3], Hong Jiang[3], Qing Chang[1], Sangeetha M. Reddy[6], Wei-Shen Chen[1,2], Michael T. Tetzlaff[2], Russell J. Broaddus[2], Michael A. Davies[7], Jeffrey E. Gershenwald[3], Lauren Haydu[3], Alexander J. Lazar[2,5], Sapna P. Patel[7], Patrick Hwu[7], Wen-Jen Hwu[7], Adi Diab[7], Isabella C. Glitza[7], Scott E. Woodman[7], Luis M. Vence[8], Ignacio I. Wistuba[5], Rodabe N. Amaria[7], Lawrence N. Kwong[5], Victor Prieto[2], R. Eric Davis[9], Wencai Ma[9], Willem W. Overwijk[7], Arlene H. Sharpe[10], Jianhua Hu[4], P. Andrew Futreal[1], Jorge Blando[5], Padmanee Sharma[8,11], James P. Allison[8], Lynda Chin[1], and Jennifer A. Wargo[1,3]

ABSTRACT

Immune checkpoint blockade represents a major breakthrough in cancer therapy; however, responses are not universal. Genomic and immune features in pretreatment tumor biopsies have been reported to correlate with response in patients with melanoma and other cancers, but robust biomarkers have not been identified. We studied a cohort of patients with metastatic melanoma initially treated with cytotoxic T-lymphocyte–associated antigen-4 (CTLA4) blockade ($n = 53$) followed by programmed death-1 (PD-1) blockade at progression ($n = 46$), and analyzed immune signatures in longitudinal tissue samples collected at multiple time points during therapy. In this study, we demonstrate that adaptive immune signatures in tumor biopsy samples obtained early during the course of treatment are highly predictive of response to immune checkpoint blockade and also demonstrate differential effects on the tumor microenvironment induced by CTLA4 and PD-1 blockade. Importantly, potential mechanisms of therapeutic resistance to immune checkpoint blockade were also identified.

SIGNIFICANCE: These studies demonstrate that adaptive immune signatures in early on-treatment tumor biopsies are predictive of response to checkpoint blockade and yield insight into mechanisms of therapeutic resistance. These concepts have far-reaching implications in this age of precision medicine and should be explored in immune checkpoint blockade treatment across cancer types. *Cancer Discov; 6(8); 827–37. ©2016 AACR.*

See related commentary by Teng et al., p. 818.

[1]Department of Genomic Medicine, The University of Texas MD Anderson Cancer Center, Houston, Texas. [2]Department of Pathology, The University of Texas MD Anderson Cancer Center, Houston, Texas. [3]Department of Surgical Oncology, The University of Texas MD Anderson Cancer Center, Houston, Texas. [4]Department of Biostatistics, The University of Texas MD Anderson Cancer Center, Houston, Texas. [5]Department of Translational Molecular Pathology, The University of Texas MD Anderson Cancer Center, Houston, Texas. [6]Department of Cancer Medicine, The University of Texas MD Anderson Cancer Center, Houston, Texas. [7]Department of Melanoma Medical Oncology, The University of Texas MD Anderson Cancer Center, Houston, Texas. [8]Department of Immunology, The University of Texas MD Anderson Cancer Center, Houston, Texas. [9]Department of Lymphoma/Myeloma, The University of Texas MD Anderson Cancer Center, Houston, Texas. [10]Department of Microbiology and Immunobiology, Harvard Medical School, Boston, Massachusetts. [11]Genitourinary Medical Oncology, The University of Texas MD Anderson Cancer Center, Houston, Texas.

Note: Supplementary data for this article are available at Cancer Discovery Online (http://cancerdiscovery.aacrjournals.org/).

P.-L. Chen and W. Roh contributed equally to this article.

A. Reuben and Z.A. Cooper contributed equally to this article.

L. Chin and J.A. Wargo share senior authorship of this work.

Current address for Z.A. Cooper: MedImmune, Gaithersburg, Maryland.

Corresponding Author: Jennifer A. Wargo, The University of Texas MD Anderson Cancer Center, 1515 Holcombe Boulevard, FCT17.6060, Houston, TX 77030. Phone: 713-745-1553; Fax: 713-745-2436; E-mail: JWargo@mdanderson.org

doi: 10.1158/2159-8290.CD-15-1545

INTRODUCTION

Major advances have been made in the treatment of metastatic melanoma through the use of immune checkpoint blockade, with the FDA approval of numerous therapeutic regimens within the past several years (1–6) and many more being studied in clinical trials (7, 8). Treatment with immune checkpoint inhibitor monotherapy [such as monoclonal antibodies targeting cytotoxic T-lymphocyte–associated antigen-4 (CTLA4) and programmed death-1 (PD-1)] is associated with response rates of 8% to 44%, and many of these responses are durable (i.e., >2 years). However, the majority of patients do not respond to these regimens as monotherapy, and some patients develop significant toxicity (2, 9–11), particularly when these regimens are combined (4). Given these complexities, a critical need exists to identify biomarkers that accurately predict which patients will benefit from this form of therapy.

Although several genomic and immune predictors of response have been reported based on analysis of pretreatment tumor biopsies, these biomarkers are not very robust, and there is significant overlap between responders and nonresponders to therapy for the markers tested (12–15). Genomic and RNA-based studies exploring predictors of outcome to immune checkpoint blockade in melanoma suggest that tumor-specific mutational load and neoantigen signature as well as cytolytic activity are significantly associated with clinical benefit and increased overall survival (13, 16, 17). IHC-based studies also support the notion that $CD8^+$, $CD4^+$, $PD\text{-}1^+$, and programmed death-ligand 1–positive ($PD\text{-}L1^+$) cell densities in pretreatment biopsies can predict response to therapy (14, 15). However, cumulative evidence from these studies suggests that these biomarkers are not perfectly predictive (13, 14), and better biomarkers are clearly needed to optimize therapeutic decisions.

In addition to identifying predictors of response to immune checkpoint blockade, there is growing interest in understanding the mechanistic differences between different forms of immune checkpoint blockade. Transcriptome and pathway analysis using purified human T cells and monocytes from patients on either CTLA4 or PD-1 blockade demonstrates distinct gene expression profile and immunologic effects between these forms of therapy (18, 19). Whereas CTLA4 blockade induces a proliferative signature in memory T cells, PD-1 blockade leads to changes in genes implicated in cytolysis and natural killer cell function (19). This notion is further supported by animal models that demonstrate differential effects of CTLA4 and PD-1 blockade therapies on the transcriptional profiles of tumor-infiltrating $CD8^+$ T cells, with increased NFAT–JAK–STAT signaling, cell proliferation/cell cycle, and activation of effector T-cell pathways seen in CTLA4 blockade versus changes in IL2 signaling, response to type I IFN, and metabolic pathways seen in PD-1 blockade (18).

Along with this, there is a critical need to identify mechanisms of therapeutic resistance to immune checkpoint inhibitors that are potentially actionable. Groups have begun to study this (17, 20), and there is evidence that somatic mutations in antigen processing and presentation as well as upregulation of genes involved in cell adhesion, angiogenesis, and extracellular matrix remodeling may contribute to immune escape in cancer (21). In addition, molecular analyses of human melanoma samples and animal models also suggest that tumor-intrinsic oncogenic signals related to the WNT/β-catenin signaling pathway may mediate cancer immune evasion and resistance to immunotherapy, including CTLA4- and PD-1–based therapy (22).

In this study, we sought to address each of these areas of critical need by studying a unique cohort of patients with metastatic melanoma who were initially treated with CTLA4 blockade and were then treated with PD-1 blockade at time of progression. A deep immune analysis of longitudinal tumor samples was performed, yielding insights into biomarkers of response, mechanistic differences between each of these forms of therapy, and means of therapeutic resistance to immune checkpoint blockade.

RESULTS

Patient Cohort, Checkpoint Blockade Treatment, and Longitudinal Tumor Biopsies

To explore differential changes in the tumor microenvironment in distinct forms of immune checkpoint blockade, we assembled a unique cohort of 53 patients with metastatic melanoma who were initially treated with CTLA4 blockade and were then treated with PD-1 blockade if they did not respond or progressed on therapy. The scheme of treatment and longitudinal tumor sampling is shown in Fig. 1A. Biopsies were obtained (when available) prior to initiation of CTLA4 blockade, on-treatment, and after restaging in patients who did not respond to or who progressed on therapy. Clinical responders were defined by radiographic evidence of absent disease, stable disease, or decreased tumor volume for >6 months. Nonresponders were defined by tumor growth on serial CT scans after the initiation of treatment or any clinical benefit lasting ≤6 months (minimal benefit; ref. 13). Nonresponders to CTLA4 blockade were then treated with PD-1 blockade therapy, and additional biopsies were obtained early during the course of therapy and late on-treatment in nonresponders (or progressors) on PD-1 blockade (Fig. 1A). Among the patients treated with CTLA4 blockade, 13% achieved clinical benefit, whereas 87% did not, consistent with published response rates (1, 11). Supplementary Table S1A and B shows the clinical and demographic characteristics of the patients in this cohort. Available biopsies were subsequently processed for downstream immune profiling by IHC and gene expression studies (Supplementary Table S1C and S1D).

Immune Profiling in Early On-Treatment Biopsies Is Predictive of Response to CTLA4 Blockade in a Unique Cohort of Patients Treated with Sequential CTLA4 and PD-1 Blockade

The profile and kinetics of immune cell infiltrates in the tumor microenvironment were first investigated via a 12-marker IHC panel (Supplementary Table S2). At the pretreatment time point, there was no difference in any of the measured markers between responders versus nonresponders to CTLA4 blockade (Fig. 1B–D; Supplementary Fig. S1A–S1I), consistent with previous reports (23). However, analysis of early on-treatment tumor biopsies identified a significantly higher density of $CD8^+$ T cells in responders versus nonresponders to CTLA4 blockade (Fig. 1B; $P < 0.05$). IHC for other immune and immunomodulatory markers at the on-treatment time point on CTLA4 blockade showed no

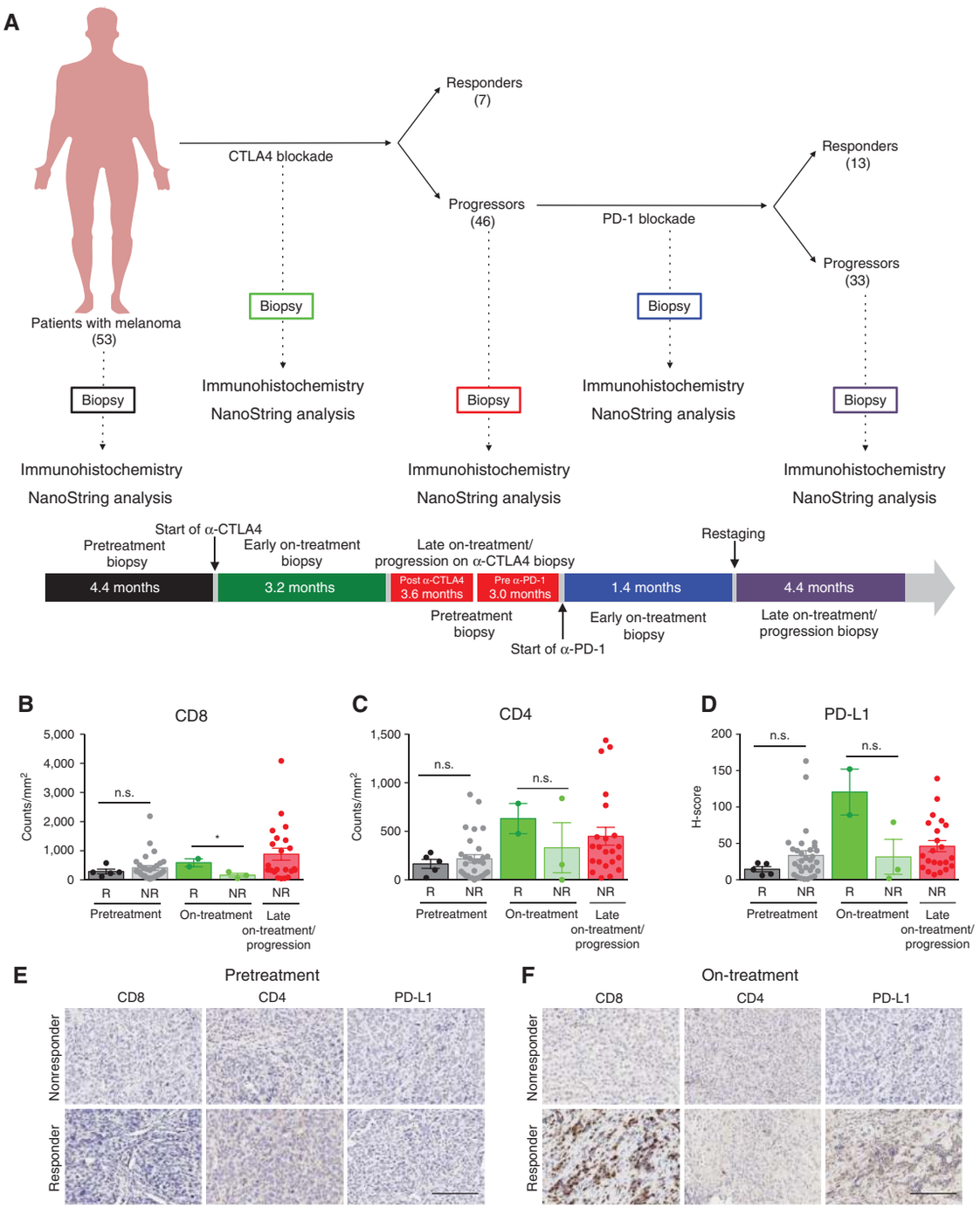

Figure 1. Immune profiling in early on-treatment biopsies is predictive of response to CTLA4 blockade in a unique cohort of patients treated with sequential CTLA4 and PD-1 blockade. **A,** patients with metastatic melanoma were initially treated with CTLA4 blockade ($n = 53$) and nonresponders to CTLA4 blockade were then treated with PD-1 blockade ($n = 46$; Expanded Access Program for MK-3475 at the MD Anderson Cancer Center). Of these 46 patients, 13 responded to PD-1 blockade, whereas 33 progressed. Tumor biopsy samples were collected at multiple time points during their treatment when feasible, including pretreatment, on-treatment, and progression anti–CTLA4 biopsies, and pretreatment, on-treatment (doses 2–3), and progression anti–PD-1 biopsies, for downstream immune profiling by IHC and gene expression studies. The median elapsed time between tumor biopsies and treatment is shown for each time point. The profile and kinetics of immune cell infiltrates in the tumor microenvironment were compared between responders and nonresponders to CTLA4 blockade. Tumor samples available for immune profiling by IHC included pretreatment anti-CTLA4 [$n = 36$; 5 responders (R) and 31 nonresponders (NR)], on-treatment anti-CTLA4 ($n = 5$; 2 responders and 3 nonresponders) and progression anti-CTLA4 biopsies ($n = 22$). CD8 (**B**) and CD4 density (**C**), and PD-L1 H-score (**D**) in responders versus nonresponders on CTLA4 blockade are shown. Representative images at pretreatment (**E**) and early on-treatment (**F**) time points are shown in responders versus nonresponders to CTLA4 blockade (20× magnification). Error bars, SEM. *, $P \le 0.05$; n.s., not significant. Scale bars, 200 μm.

significant differences in responders versus nonresponders, though a trend toward higher PD-L1 expression was observed in responders (Fig. 1C; Supplementary Fig. S1). Representative IHC images for CD8, CD4, and PD-L1 expression in responders and nonresponders to CTLA4 blockade are shown for each time point in Fig. 1E–F.

In addition, to better understand the contribution of myeloid–T cell interactions to therapeutic response, we also stained sections with additional myeloid markers (Supplementary Table S3). Though we saw no clear quantitative differences in any of the myeloid subsets in responders versus nonresponders to CTLA4 blockade (Supplementary Fig. S2A–S1H), we observed a slightly higher proximity of $CD68^+$ myeloid cells to $CD8^+$ T cells in nonresponders at the pretreatment time point (Supplementary Fig. S3A and S1B; $P = 0.08$); however, this did not reach statistical significance in this small cohort.

Immune Profiling in Early On-Treatment Biopsies Is Highly Predictive of Response to PD-1 Blockade

We next used our 12-marker IHC panel to interrogate the profiles and kinetics of immune cell subsets in tumor samples from patients on anti–PD-1 therapy. Forty-six patients were included who were initially treated with CTLA4 blockade, as well as 11 additional patients who had not received prior CTLA4 blockade to control for possible prior CTLA4 blockade exposure effects. In these studies, we observed a modest but statistically significant difference in the density of $CD8^+$, $CD3^+$, and $CD45RO^+$ T cells in pretreatment samples of responders compared with nonresponders (Fig. 2A–F; Supplementary Fig. S4A; $P = 0.03$, 0.03, 0.02, respectively), though the values between these two groups were largely overlapping, consistent with prior published data (23). There was also a trend toward higher pretreatment expression of CD4 and PD-1 in responders versus nonresponders, though these did not reach statistical significance (Fig. 2A–F; $P = 0.06$, $P = 0.08$, respectively).

In contrast, there was a profound and highly statistically significant difference in the expression of markers for T-cell subsets—CD8 ($P = 0.001$), CD4 ($P = 0.001$), and CD3 ($P < 0.001$)—and immunomodulatory molecules PD-1 ($P < 0.001$), PD-L1 ($P = 0.007$), and LAG3 ($P < 0.0001$) in responders versus nonresponders to therapy in early on-treatment tumor samples, with little to no overlap between groups (Fig. 2A–F). Of note, a significantly higher level of expression of FOXP3 ($P < 0.001$) and granzyme B ($P = 0.02$) was observed in responders compared with nonresponders to therapy, likely relating to an enhanced activation status of infiltrating T cells in responding patients (Supplementary Fig. S4A–S4F). Importantly, these changes were observed in responders as early as 2 to 3 doses following initiation of PD-1–based therapy. Representative IHC images for these markers are shown in Fig. 2G and H. Specific analysis performed on longitudinal samples also demonstrated an increase in CD8, PD-1, and PD-L1 in responders compared with nonresponders to PD-1–based therapy (Supplementary Fig. S5A–S5F).

In light of previous studies demonstrating the importance of the invasive tumor margin in predicting responses to PD-1 blockade (14), we quantified $CD8^+$ T-cell density at the tumor margin in 41 samples with discernible tumor margins. In these studies, we did not observe significant differences in $CD8^+$ T cells at the tumor margin between responders and nonresponders to PD-1–based therapy at all time points examined, though sample size was admittedly limited. However, when we compared the ratio of $CD8^+$ T cells at tumor center versus the margin in early on-treatment biopsies, we observed significantly higher ratios of $CD8^+$ T cells at the tumor center versus the margin within responders compared with nonresponders (Supplementary Fig. S6A–S6H), suggesting possible infiltrate from margin to center of the tumor in the context of therapy.

To augment these studies, we performed immune profiling in the separate cohort of patients who received PD-1 blockade in the absence of prior CTLA4 exposure, and observed no significant differences in our prior observations when these patients were included in the analysis (Supplementary Fig. S7A–S7H; Supplementary Table S4). As observed previously with CTLA4 blockade, we saw no clear quantitative difference in any of the myeloid subsets in responders and nonresponders to PD-1 blockade (Supplementary Fig. S8A–S8I). However, we observed a significantly higher proximity of $CD68^+$ myeloid cells to $CD8^+$ T cells in nonresponders at the pretreatment and on-treatment time points for patients on PD-1 blockade (Supplementary Fig. S3, $P < 0.05$).

Gene Expression Profiling in Longitudinal Tumor Biopsies Is Predictive of Response in Patients Treated with Sequential CTLA4 and PD-1 Blockade

To further dissect the tumor microenvironment–mediated response and resistance to immune checkpoint blockade and to identify potential mechanisms of therapeutic resistance, we performed targeted gene expression profiling (GEP) via a custom 795-gene NanoString panel composed of immune-related genes and genes pertaining to common cancer signaling pathways (Supplementary Table S5) in samples with available tissue. When comparing GEP results between responders and nonresponders at each individual biopsy time point, no significant differences were found at pretreatment CTLA4 blockade, on-treatment CTLA4 blockade, and pretreatment PD-1 blockade. However, early on-treatment tumor samples of patients on anti–PD-1 therapy showed 411 significantly differentially expressed genes (DEG) in responders (FDR-adjusted $P < 0.05$), mostly upregulated as compared with nonresponders (Fig. 3A–D; Supplementary Fig. S9 and Supplementary Table S6A–S6E), including IHC markers represented in the NanoString codeset, cytolytic markers, HLA molecules, IFNγ pathway effectors, chemokines and select adhesion molecules. Notably, a small number of DEGs ($n = 6$) were lower in responders than in nonresponders on PD-1 blockade and included vascular endothelial growth factor (*VEGFA*), suggesting a mechanism of therapeutic resistance and a potential target for therapy, which is corroborated by data from others implicating angiogenesis in resistance to immunotherapy (24–26). Notably, though only 10 of the 12 IHC markers were represented in the NanoString codeset, all 10 overlapping probes showed concordance with our IHC findings (Supplementary Fig. S10A–S10J and S11A–S11J).

We next compared GEPs between pretreatment and on-treatment time points to identify dynamic changes in the tumor microenvironment associated with each form of immune checkpoint therapy. To do this, we used the linear mixed-effects model to test time trend of gene expression from pretreatment to on-treatment and its interaction with response status for CTLA4 and PD-1 blockade, respectively. With CTLA4 blockade, 173 upregulated DEGs and

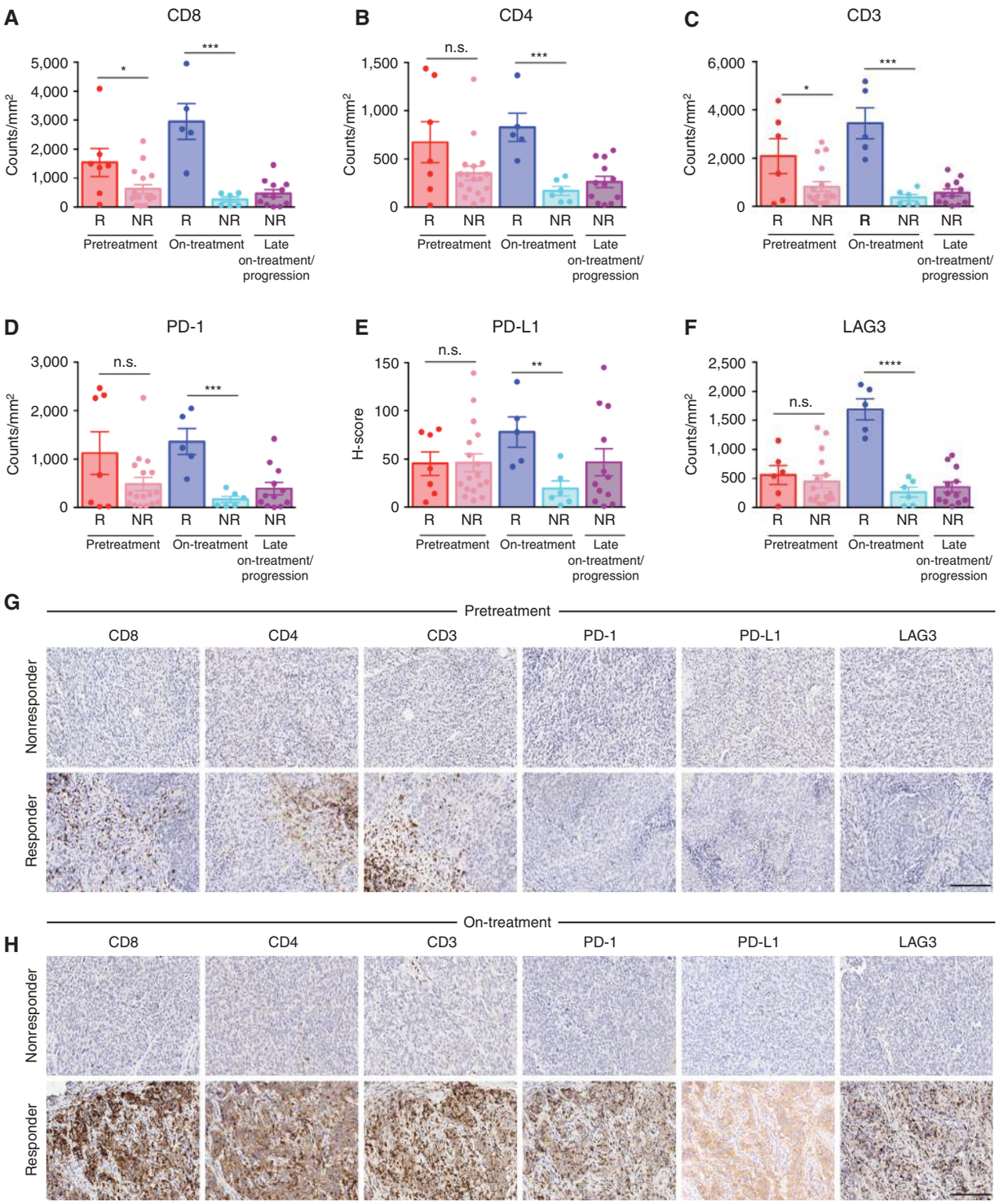

Figure 2. Immune profiling in early on-treatment biopsies is highly predictive of response to PD-1 blockade. Longitudinal tumor biopsies were performed (at pretreatment, early on-treatment, and late on-treatment/progression time points) in patients undergoing treatment with PD-1 blockade ($n = 47$). The profile and kinetics of immune cell infiltrates in the tumor microenvironment were compared between responders (R) and nonresponders (NR) to PD-1 blockade. Tumor samples available for immune profiling by IHC included pretreatment anti–PD-1 ($n = 24$; 7 responders and 17 nonresponders), on-treatment anti–PD-1 (doses 2–3; $n = 11$; 5 responders and 6 nonresponders), and progression anti–PD-1 ($n = 12$) biopsies (Supplementary Table S1C). CD8 (**A**), CD4 (**B**), CD3 (**C**), PD-1 (**D**), PD-L1 (H-score) (**E**), and LAG3 (**F**) density are shown in responders versus nonresponders. Representative images at pretreatment (**G**) and early on-treatment (**H**) time points are shown in responders versus nonresponders to PD-1 blockade (20× magnification). Error bars, SEM. *, $P \le 0.05$; **, $P \le 0.01$; ***, $P \le 0.001$; ****, $P \le 0.0001$; n.s., not significant. Scale bars, 200 μm.

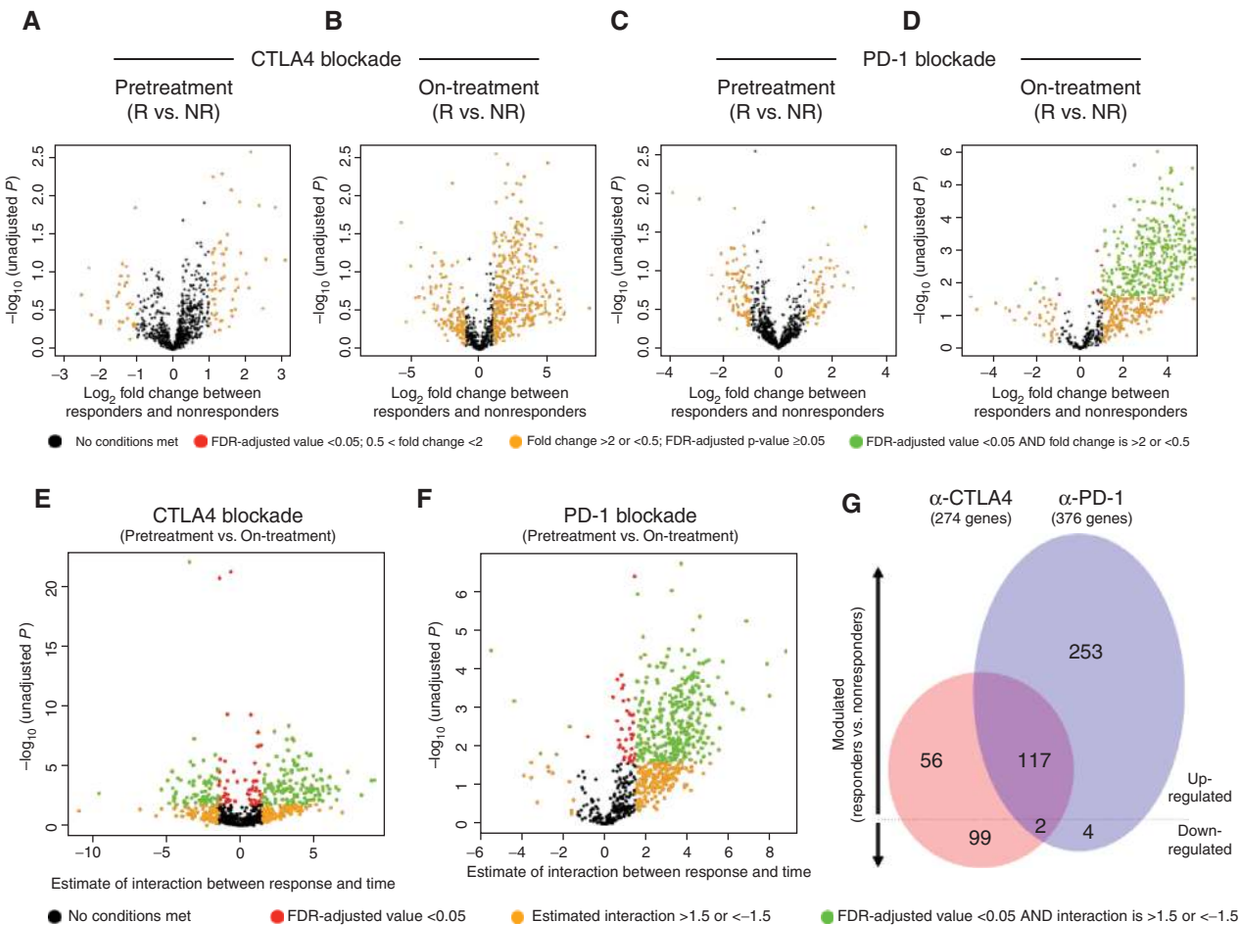

Figure 3. Gene expression profiling in longitudinal tumor biopsies is predictive of response in a unique cohort of patients treated with sequential CTLA4 and PD-1 blockade. Gene expression profiling was performed via NanoString in longitudinal tumor biopsies from patients treated with sequential CTLA4 and PD-1 blockade ($n = 54$), including pretreatment anti–CTLA4 [$n = 16$; 5 responders (R) and 11 nonresponders (NR)], on-treatment anti-CTLA4 ($n = 5$; 3 responders and 2 nonresponders), and progression anti–CTLA4 biopsies ($n = 15$), pretreatment anti–PD-1 ($n = 16$; 7 responders and 9 nonresponders), on-treatment anti–PD-1 (doses 2–3; $n = 10$; 5 responders and 5 nonresponders), and progression anti–PD-1 ($n = 7$) biopsies (Supplementary Tables S1D, S6A, and S9B–S9C). Volcano plots illustrate the $\log_2$ fold change (FC) in gene expression (responders vs. nonresponders) on the x-axis and unadjusted *P* values from Student *t* tests between responders and nonresponders on the y-axis. Differentially expressed genes (FDR-adjusted $P < 0.05$ and FC >2 or <−1/2) between responders and nonresponders were highlighted in green at the time of pretreatment (**A**) and on-treatment (**B**) CTLA4 blockade, pretreatment (**C**) and on-treatment (**D**) PD-1 blockade. Interaction of time covariate (pretreatment, on-treatment) and response covariate (responders, nonresponders) was illustrated in volcano plots. Genes with significant interaction were highlighted in green (FDR-adjusted $P < 0.05$ and interaction >1.5 or <−1.5) for CTLA4 blockade (**E**) and PD-1 blockade (**F**). Venn diagram illustrates shared and unique genes upregulated and downregulated in CTLA4 (red) and PD-1 (blue) blockade over treatment time course (**G**).

101 downregulated DEGs were identified in responders versus nonresponders to therapy (Fig. 3E; Supplementary Table S7), with upregulated DEGs similar to those described in previously published datasets (18). With PD-1 blockade, 370 upregulated DEGs and 6 downregulated DEGs were identified in responders versus nonresponders (Fig. 3F; Supplementary Table S8). Upregulated DEGs related to processes such as antigen presentation, T-cell activation, and T-cell homing. Importantly, we did not observe significant differences in GEPs in PD-1–treated patients regardless of prior treatment with CTLA4 blockade (Supplementary Fig. S12; Supplementary Table S9A–S9C); however, the cohort was admittedly small and we cannot exclude the possibility that these GEPs may in part be due to prior treatment with CTLA4 blockade.

To investigate mechanistic differences between the two forms of immune checkpoint blockade, we next compared the response-associated DEGs (from pretreatment to on-treatment) in tumor biopsies of CTLA4- versus PD-1–treated patients. In this comparison, only 117 shared DEGs were upregulated for both CTLA4 and PD-1 blockade (Fig. 3G), with 56 upregulated DEGs unique to CTLA4 blockade, and 253 unique to PD-1 blockade (FDR-adjusted $P < 0.05$; Supplementary Table S10). Analysis of shared downregulated DEGs revealed 99 that were unique to CTLA4 blockade and 4 that were unique to PD-1 blockade (FDR-adjusted $P < 0.05$; Supplementary Table S10), with only two common DEGs in responders versus nonresponders across both forms of therapy, including dual serine/threonine and tyrosine protein kinase (*DSTYK*) and S100 Calcium Binding Protein A1 (*S100A1*).

To complement these studies and to explore the dynamic changes in GEP between responders and nonresponders over the course of checkpoint blockade therapy, we compared

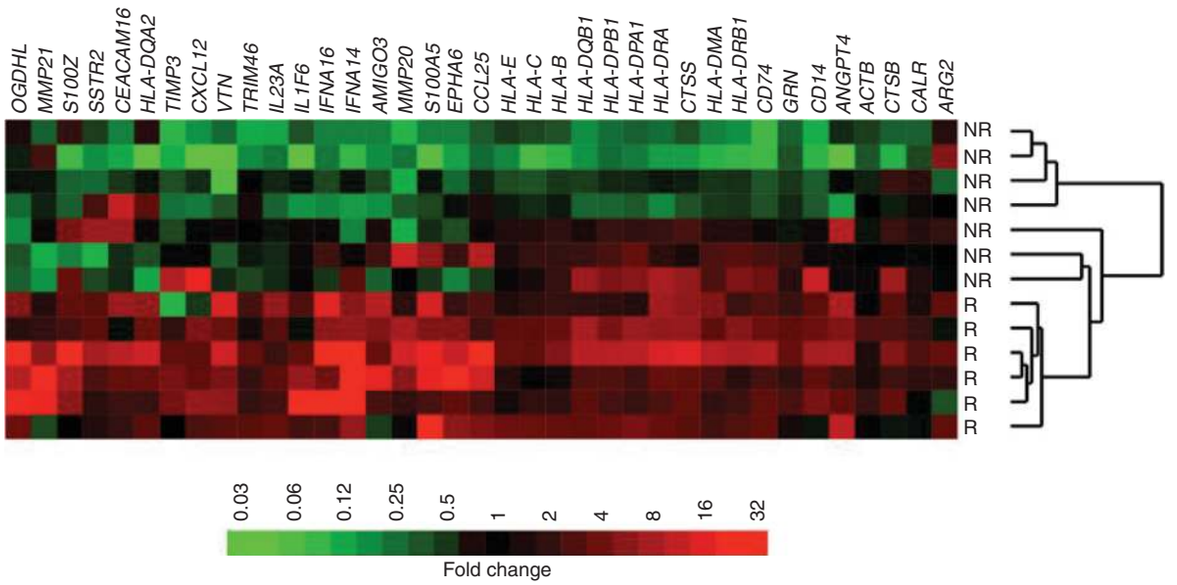

Figure 4. NanoString paired analysis. For analysis of paired samples, raw NanoString counts were compared between samples after anti–PD-1 therapy with those in the corresponding pretreatment sample. Shown are the 37 genes most frequently upregulated in responders (R) and/or downregulated in nonresponders (NR), identified by paired analysis.

GEP results for paired (same-patient) biopsies taken before and after PD-1 blockade. Heat mapping of the fold change between paired biopsies for the 37 genes most frequently upregulated in responders and/or downregulated in nonresponders ("Up-DEGs") clustered responders separately from nonresponders (Fig. 4; Supplementary Table S11A–S11B). Pathway analysis of Up-DEGs showed that response to PD-1 blockade involves an adaptive immune response, with increased expression of antigen presentation molecules and markers of T-cell activation in responding patients. Interestingly, many Up-DEGs were actually downregulated in on-treatment samples of nonresponders compared with pretreatment, including interferon and HLA genes.

DISCUSSION

Immune checkpoint blockade therapies have revolutionized the treatment of advanced melanoma and other cancer types; however, only a fraction of patients benefit from these treatments as monotherapy, and robust predictors of response and mechanisms of therapeutic resistance are currently lacking. Though data suggest a correlation among clinical response, preexisting tumor-infiltrating lymphocytes, T-cell repertoire, tumor-intrinsic mutational load, and neoantigens, the demonstrated biomarker profiles between responders and nonresponders are often overlapping and not very robust (9, 15).

Together, the studies presented herein build on collective efforts to identify biomarkers of response and resistance to immune checkpoint blockade (13–15), and provide novel evidence that assessment of adaptive immune responses early in the course of therapy is highly predictive of response—with nonoverlapping immune signatures in responders versus nonresponders, particularly to PD-1 blockade. These data have important clinical implications and suggest that immune signatures in tumor biopsies should be evaluated early after initiation of treatment with immune checkpoint blockade rather than in pretreatment tumor samples—at least until better predictive markers in pretreatment tissue and blood samples may be identified. This is highly relevant, as many clinical trials of immune checkpoint inhibitors currently mandate assessment of immune markers only in pretreatment tumor tissue; however, our findings suggest that we should reconsider this approach and assess adaptive immune responses in patients on therapy. Of note, we recognize the immune signatures observed in early on-treatment samples may simply be a consequence of the immune response to checkpoint inhibitors, and may not represent bona fide mechanisms of therapeutic response. Additional studies are needed to fully delineate whether these immune signatures are responsible for, or a product of, the mechanisms underlying the response—though are admittedly out of the context of the current study. Importantly, similar observations have been made in other tumor types (27), suggesting that such an approach could be applicable to other solid tumors—though this hypothesis needs to be tested more broadly.

These data also offer mechanistic insight into response to immune checkpoint blockade, suggesting that response to PD-1 blockade is related to enhanced cytolytic activity, antigen processing, and IFNγ pathway components (16, 17). Interestingly, *VEGFA* was decreased in responders and increased in nonresponders to therapy, suggesting a mechanism of therapeutic resistance as observed by others (24–26) and a potential target for therapy. The antiangiogenesis pathway has been shown to interact with antitumor immunity through multiple mechanisms. Previous studies demonstrate that increased VEGF secretion decreases T-cell effector function and trafficking to tumor (28, 29) and correlates with increased PD-1 expression on CD8 T cells (25). In addition to direct effect on T cells, VEGF also decreases the number of immature dendritic cells as well as T-cell priming ability of mature dendritic cells

(30), further contributing to decreased effector T-cell function. Angiogenic factors have also been shown to expand T regulatory cell (31) and myeloid-derived suppressor cell populations. Based on these findings and preclinical and translational data supporting synergy between angiogenesis inhibitors and immunotherapies, multiple trials of combination therapy are under way, including bevacizumab with anti–PD-1 therapy (26). Phase I trial data from patients with advanced melanoma of bevacizumab and ipilimumab support synergy with this combination therapy, showing a 67% disease control rate, increased CD8 T-cell tumor infiltration, and circulating memory CD4 and CD8 T cells with combination therapy (26, 32). Our data are in line with these studies and reinforce the value in these combination anti-VEGF/anti–PD-1 clinical trials.

In addition, these data provide strong evidence regarding differential effects of distinct forms of immune checkpoint blockade on the tumor microenvironment, with insight into distinct mechanisms of response and of therapeutic resistance, which is in line with prior published reports in mice (18) and in humans (19). These differences have important clinical implications and may help guide rational therapeutic combinations of distinct immune checkpoint inhibitors and immunomodulatory agents depending on the desired treatment effect.

Finally, these studies offer novel insight into mechanisms of therapeutic resistance to immune checkpoint blockade which may be potentially actionable. Examples highlighted by these data include an angiogenic phenotype in nonresponding lesions (24, 33), as well as downregulation of antigen processing and presentation (including HLA; refs. 34, 35), and defects in interferon signaling pathways (36). These data are also supported by The Cancer Genome Atlas recent study demonstrating enrichment of mutations in antigen presentation machinery (including HLA and β2-m) as well as extrinsic apoptotic genes in preventing cytotoxic cells from killing tumor cells (21). Importantly, many of these mechanisms may be targetable and could help overcome therapeutic resistance to immune checkpoint blockade.

Despite these provocative results, several limitations exist with these studies. Our sample size in the current study is admittedly limited; however, similar findings have been observed in other histologies (27), and efforts to expand this cohort are ongoing. In addition and potentially related to the limited sample size, robust biomarkers were not identified in pretreatment samples, which is in contrast to other published reports (14). However, this disparity could also be related to different antibodies used for the markers in question (namely PD-L1).

An important consideration is that the differences in immune infiltrates observed in responders versus nonresponders to PD-1–based therapy could be related to prior treatment with CTLA4 blockade, though gene expression analyses and IHC results in CTLA4-naïve versus CTLA4-experienced patients did not differ significantly. This cohort is admittedly small and results need to be validated in larger cohorts and in other histologies. Based on available data from this and other groups, biopsies should be performed early on treatment (i.e., within 2 to 3 cycles of therapy) to validate these studies. In addition, though these novel findings are provocative, they may be difficult to validate in other solid tumor types where acquisition of early on-treatment biopsies may be less feasible. Nonetheless, there is a critical need to study this phenomenon in other solid tumors, as results from such studies may help usher in a new paradigm for immune monitoring in the setting of immune checkpoint blockade—with emphasis placed on assessment of an adaptive immune response in an early on-treatment biopsy rather than in pretreatment markers.

METHODS

Patient Cohort

An initial cohort of 53 patients with metastatic melanoma were included in this study. These patients were treated at The University of Texas (UT) MD Anderson Cancer Center between October 2011 and March 2015 and had tumor samples collected and analyzed under Institutional Review Board (IRB)–approved protocols (IRB LAB00-063, LAB03-0320, 2012-0846, PA13-0291, and PA12-0305). Of note, these studies were conducted in accordance with the Declaration of Helsinki and approved by the UT MD Anderson Cancer Center IRB. Electronic medical charts were reviewed independently by two investigators to assign clinical response group and document other clinical parameters (Supplementary Table S1A and S1B). These 53 patients were initially treated with CTLA4 blockade, with 7 responding whereas 46 progressed. The 46 patients who progressed on CTLA4 blockade then went on to receive PD-1 blockade therapy (Expanded Access Program for MK-3475 at the MD Anderson Cancer Center). Of these 46 patients, 13 responded to PD-1 blockade, whereas 33 progressed. In addition, a separate cohort of 16 CTLA4 blockade-naïve patients were also included in this study and received PD-1 blockade only. Of these 16 patients, 12 responded and 4 progressed. Altogether, a total of 62 patients received anti–PD-1 treatment (both CTLA4 blockade–treated and CTLA4 blockade–naïve); 25 responded (40%) and 37 progressed (60%). Of note, in this study one patient received CTLA4 blockade and progressed but did not go on to receive PD-1 blockade therapy. Clinical response (responders) was defined by radiographic evidence of freedom from disease, stable disease, or decreased tumor volume for more than 6 months. Lack of a clinical response (nonresponders) was defined by tumor growth on serial CT scans or a clinical benefit lasting 6 months or less (minimal benefit).

Tumor Samples

Tumor samples were obtained from the MD Anderson Cancer Center Department of Pathology archive and Institutional Tumor Bank with appropriate written informed consent. Biopsy collection and analyses were approved by the MD Anderson Cancer Center IRB (LAB00-063, LAB03-0320, 2012-0846, PA13-0291, and PA12-0305). Tumor biopsy samples were collected at multiple time points during treatment when feasible, including pretreatment, on-treatment and progression anti-CTLA4 biopsies, and pretreatment, on-treatment (doses 2–3), and progression anti–PD-1 biopsies. Biopsy sites were chosen as follows: for pretreatment and early on-treatment biopsies, the most safely accessible tumors were biopsied; for progression biopsies, progressing tumors were sampled. The median times for pretreatment, on-treatment, and progression anti-CTLA4 biopsies were 4.4 months prior (0–59.3 months, average 9.2 months), 3.2 months after (0.1–16.8 months, average 4.6 months), and 3.6 months after (0.2–38.5 months, average 8.0 months) anti-CTLA4 treatment, respectively. The median times for pretreatment, on-treatment, and progression anti–PD-1 biopsies were 3.0 months prior (0–35 months, average 6 months), 1.4 months after (0.7–26 months, average 4.5 months), and 4.4 months after (1.6–320 months, average 5 months) anti–PD-1 treatment, respectively. All specimens were excisional biopsies or surgical resection specimens. For the 16 CTLA4 blockade–naïve patients, the median times for pretreatment and on-treatment anti–PD-1 biopsies were 2.1 months prior and 2.8 months after, respectively, and tumor samples were excisional biopsies or surgical resection specimens.

Immune Profiling by IHC

Tumor samples ($n = 88$) were formalin-fixed and paraffin-embedded, including pretreatment anti–CTLA4 ($n = 36$; 5 responders and 31 nonresponders), on-treatment anti-CTLA4 ($n = 5$; 2 responders and 3 nonresponders), progression anti-CTLA4 ($n = 22$), pretreatment anti–PD-1 ($n = 24$; 7 responders and 17 nonresponders), on-treatment anti–PD-1 (doses 2–3; $n = 11$; 5 responders and 6 nonresponders), and progression anti–PD-1 ($n = 12$) biopsies (Supplementary Table S1C). To examine the effect of CTLA4 blockade on pretreatment and on-treatment PD-1 blockade biopsies, additional immune profiling analysis by IHC was performed on a separate cohort of patients treated with PD-1 blockade who were CTLA4 blockade–naïve ($n = 13$), including pretreatment anti–PD-1 ($n = 9$; 7 responders and 2 nonresponders) and on-treatment anti–PD-1 ($n = 4$; 2 responders and 2 nonresponders) biopsies. From each tissue block, a hematoxylin and eosin–stained slide was examined to evaluate tumor cellularity. IHC was performed using an automated stainer (Leica Bond Max, Leica Biosystems), and the primary antibodies used included CD3 (DAKO, A0452, 1:100), CD4 (Leica Biosystems, NCL368, 1:80), CD8 (Thermo Scientific MA5-13473, 1:25), CD20 (DAKO, L26, 1:1,400), CD45RO (Leica Biosystems, PA0146, ready to use), CD57 (BD Biosciences, 347390, 1:40), CD68 (DAKO, MO876, 1:450), FOXP3 (BioLegend, 320102, 1:50), Granzyme B (Leica Microsystems, PA0291, ready to use), LAG3 (LifeSpan Bioscience, 17B4, 1:100), PD-1 (Epitomics, ab137132, 1:250), PD-L1 (Cell Signaling Technology, 13684, 1:100), CD14 (Abcam, Ab133503, 1:100), CD33 (Leica Microsystems, LCD33-L-CE, 1:100), CD163 (Leica Biosystems, NCL-L-CD163, 1:500), and CD206 (Abcam, Ab64693, 1:2,000). All slides were stained using previously optimized conditions with appropriate positive and negative controls. The IHC reaction was detected using the Leica Bond Polymer Refine detection kit (Leica Biosystems) and diaminobenzidine (DAB) was used as chromogen. Counterstaining was done using hematoxylin. IHC and hematoxylin and eosin–stained slides were converted into high-resolution digital images using an Aperio slide scanner (Aperio AT Turbo, Leica Biosystems). The digital images were then analyzed using the Aperio Image Toolbox analysis software (Leica Biosystems), Aperio image analysis algorithms nuclear and cytoplasmic v9. From each e-slide, 5×1 mm^2 areas within the tumor region (except for small biopsy samples) were chosen by a pathologist for digital analysis. IHC staining for CD3, CD4, CD8, CD20, CD45RO, CD57, CD68, FOXP3, Granzyme B, LAG3, PD-1, CD14, CD33, CD163, and CD206 was evaluated as density of cells, defined as the number of positive cells per mm^2. PD-L1 expression was evaluated in tumor cells using H-score, which includes the percentage of positive cells showing membrane staining pattern (0–100) multiplied by the intensity of the staining (0 to 3+), with a total score ranging from 0 to 300. The final score for each marker was expressed as the average score of the areas analyzed within the tumor region (tumor center). In addition, of the initial cohort of 88 samples scored, 41 samples showing discernible tumor margins were evaluated for CD8 density at both tumor margin and center. The final scores for each marker from each patient were then transferred to a database for statistical analysis.

Immunofluorescence

For a subset of formalin-fixed and paraffin-embedded samples ($n = 19$), we performed immunofluorescence staining for CD8 (Thermo Scientific, MA5-13473) and CD68 (DAKO, MO876) to investigate potential myeloid–T cell interactions, including pretreatment anti-CTLA4 ($n = 5$; 2 responders and 3 nonresponders), on-treatment anti-CTLA4 ($n = 2$; 1 responder and 1 nonresponder), pretreatment anti–PD-1 ($n = 6$; 3 responders and 3 nonresponders), and on-treatment anti–PD-1 (doses 2–3; $n = 6$; 3 responders and 3 nonresponders) biopsies. This was done following the Opal protocol staining method with CD8 in Alexa488 (1:50) and CD68 in Alexa594 (1:100).

For quantification, each individually stained DAPI-, CD8-, and CD68-stained section was utilized to establish the spectral library of fluorophores required for multispectral analysis. Slides were scanned using the Vectra slide scanner (PerkinElmer) under fluorescent conditions. For each marker, the mean fluorescent intensity per case was then determined as a base point from which positive calls could be established. Finally, an average of five random areas on each slide were analyzed for contact quantification (ratio of number of CD68 cells in contact with CD8 divided by number of CD68 cells) blindly by a pathologist at 20× magnification.

NanoString Analysis

A subset of tumor samples ($n = 54$) with adequate tissue following immune profiling were selected for NanoString analysis using a custom-designed 795-gene codeset. All tumor samples were prepared from formalin-fixed and paraffin-embedded tissue blocks, including pretreatment anti-CTLA4 ($n = 16$; 5 responders and 11 nonresponders), on-treatment anti-CTLA4 ($n = 5$; 3 responders and 2 nonresponders), progression anti-CTLA4 ($n = 15$), pretreatment anti–PD-1 ($n = 16$; 7 responders and 9 nonresponders), on-treatment anti–PD-1 (doses 2–3; $n = 10$; 5 responders and 5 nonresponders), and progression anti–PD-1 ($n = 7$) biopsies (Supplementary Tables S1D and S5). Hematoxylin and eosin–stained sections were prepared to evaluate tumor cellularity. Total RNA was extracted from each sample individually using the RNeasy Mini Kit (QIAGEN). For each NanoString assay, 1 μg of total tissue RNA was isolated, mixed with a NanoString code set mix, and incubated at 65°C overnight (16–18 hours). The reaction mixes were loaded on the NanoString nCounter Prep Station for binding and washing, and the resulting cartridge was transferred to the NanoString nCounter digital analyzer for scanning and data collection. A total of 600 fields were captured per sample to generate the raw digital counts for each sample. To examine the effect of prior CTLA4 blockade on anti–PD-1 pretreatment and on-treatment tissue samples, a separate gene expression profiling analysis was performed using a custom-designed, 795-probe codeset on 28 samples (due to exhaustion of NanoString custom code sets used in Figs. 3 and 4; Supplementary Table S9A–S9C). Compared with the initial code set, the β2-microglobulin probe was deleted and the Melanoma Inhibitory Activity (MIA) probe was added. The same preprocessing, normalization, and statistical analysis of NanoString nCounter data were applied to these 28 anti–PD-1 samples, which included 7 pretreatment samples (4 responders, 3 nonresponders) and 8 on-treatment samples with prior CTLA4 blockade (3 responders, 5 nonresponders), as well as 8 pretreatment samples (6 responders, 2 nonresponders) and 5 on-treatment samples (2 responders, 3 nonresponders) that were CTLA4 blockade–naïve.

Statistical Analysis

Immune Profiling by IHC Analyses were performed using GraphPad Prism software. All tests were two-sided, parametric *t* tests. *P* values of <0.05 were considered statistically significant.

NanoString Data Preprocessing Raw count data were preprocessed using NanoStringNorm R package *NanoStringNorm* (37). Specifically, geometric mean–based scaling normalization was performed to account for technical assay variation, followed by background adjustment and RNA content normalization via annotated housekeeping genes. The most stable set of housekeeping genes (*ABCF1, GUSB, TBP*, and *TUBB*) was selected by the geNorm algorithm (38). Finally, $\log_2$-transformed data were used for downstream analyses (Supplementary Tables S6A and S9C). Unsupervised hierarchical clustering analysis, with heatmap shown in Supplementary Fig. S13, showed no batch effect and no significant correlations between batch, time, and clinical response.

Differential Gene Expression Analysis Fold change of each gene was calculated as the ratio of average gene expression intensity of the responder group to that of the nonresponder group. A two-sample *t* test was used to compare gene expression intensities between the responder

group and the nonresponder group. To account for multiple testing, we used FDR (39), defined as the probability of being true under null hypothesis when rejected and widely used in high-dimensional problems. The beta-uniform mixture model (40) was used to obtain FDR. A gene was claimed to be differentially expressed if it showed a fold change of >2 (increased in responders) or ≤ −1/2 (increased in nonresponders) and FDR ≤ 0.05. Volcano plots were used to visualize $\log_2$ fold change on the x-axis and *P* values on the *y*-axis. Each gene was color coded based on its fold change and FDR (Fig. 3A–D). This analysis was performed at individual time points (pre–anti-CTLA4, on–anti-CTLA4, pre–anti-PD-1, and on–anti-PD-1 treatment).

Assessment of Time-by-Response Interaction We used a linear mixed-effects model, implemented using R package *lme4*, to evaluate interactions between "Time (pretreatment, on-treatment)" and "Response (responders, nonresponders)" on gene expression intensity (41). In this model, we included time, response, and time-by-response interactions as the fixed effects and a patient-specific random intercept assumed to follow a mean 0 normal distribution. Again, an FDR threshold of 0.05 was used to select genes with significant interaction between time and response. Genes with positive interaction coefficients showed upregulated expression in responders or downregulated expression in nonresponders after a treatment, whereas genes with negative interaction coefficients showed downregulated expression in responders or upregulated expression in nonresponders after a treatment. We used volcano plots to visualize the interaction coefficients on the x-axis and *P* values on the *y*-axis. Each gene was color coded based on its interaction coefficients and FDR (Fig. 3E and F). Such an analysis was separately performed for each treatment (anti-CTLA4 and anti–PD-1 treatment).

NanoString Paired Analysis For the analysis of paired samples, raw NanoString counts were compared between samples after anti–PD-1 therapy with those in the corresponding pretreatment sample by Poisson distribution-based statistics as previously described (42). The 37 Up-DEGs identified by analysis of paired samples (Fig. 3H), comparing expression values after anti–PD-1 therapy to the value in the pretreatment sample, were analyzed by the hypergeometric distribution test (43) for enrichment of gene sets. Categories of gene sets came from the Molecular Signatures Database, Gene Ontology, the Kyoto Encyclopedia of Genes and Genomes (KEGG), and a custom collection from the scientific literature (Ma_census). Gene sets with an FDR *q* value of ≤ 0.1 are displayed.

Disclosure of Potential Conflicts of Interest

M.A. Davies reports receiving commercial research grants from GlaxoSmithKline, AstraZeneca, Merck, Oncothyreon, Sanofi Aventis, and Genentech and is a consultant/advisory board member for Novartis, GlaxoSmithKline, Genentech, Sanofi Aventis, and Vaccinex. J.E. Gershenwald is a consultant/advisory board member for Merck. S. Patel has received speakers bureau honoraria from Bristol-Myers Squibb and Merck and is a consultant/advisory board member for Genentech. A.H. Sharpe reports receiving a commercial research grant from Novartis, has ownership interest (including patents) in Roche and Bristol-Myers Squibb, and is a consultant/advisory board member for Costim. P. Sharma is a consultant/advisory board member for Bristol-Myers Squibb, Amgen, GlaxoSmithKline, and AstraZeneca. J.A. Wargo is a paid speaker at Bristol-Myers Squibb, Novartis, and Roche Genentech; reports receiving commercial research support from Bristol-Myers Squibb; has received speakers bureau honoraria from DAVA Oncology, Novartis, Bristol-Myers Squibb, Roche Genentech, and Illumina; and is a consultant/advisory board member for GlaxoSmithKline. No potential conflicts of interest were disclosed by the other authors.

Authors' Contributions

Conception and design: P.-L. Chen, W. Roh, A. Reuben, M.T. Tetzlaff, P.A. Futreal, J.P. Allison, L. Chin, J.A. Wargo

Development of methodology: P.-L. Chen, W. Roh, Z.A. Cooper, Q. Chang, A.J. Lazar, I.I. Wistuba, J.P. Allison, L. Chin, J.A. Wargo

Acquisition of data (provided animals, acquired and managed patients, provided facilities, etc.): P.-L. Chen, A. Reuben, Z.A. Cooper, C.N. Spencer, J.P. Miller, K. Wani, M.P. De Macedo, W.-S. Chen, M.T. Tetzlaff, R.J. Broaddus, M.A. Davies, J.E. Gershenwald, L. Haydu, A.J. Lazar, S.P. Patel, P. Hwu, W.-J. Hwu, L.M. Vence, I.I. Wistuba, R.N. Amaria, V. Prieto, J.P. Allison, L. Chin, J.A. Wargo

Analysis and interpretation of data (e.g., statistical analysis, biostatistics, computational analysis): P.-L. Chen, W. Roh, A. Reuben, Z.A. Cooper, P.A. Prieto, J.P. Miller, R.L. Bassett, V. Gopalakrishnan, J.E. Gershenwald, A.J. Lazar, W.-J. Hwu, A. Diab, S.E. Woodman, L.M. Vence, R.N. Amaria, L.N. Kwong, R.E. Davis, W. Ma, A.H. Sharpe, J. Hu, P.A. Futreal, J. Blando, P. Sharma, J.P. Allison, L. Chin, J.A. Wargo

Writing, review, and/or revision of the manuscript: P.-L. Chen, W. Roh, A. Reuben, Z.A. Cooper, P.A. Prieto, J.P. Miller, R.L. Bassett, V. Gopalakrishnan, J.L. Austin-Breneman, S.M. Reddy, M.T. Tetzlaff, M.A. Davies, J.E. Gershenwald, L. Haydu, A.J. Lazar, S.P. Patel, P. Hwu, W.-J. Hwu, I.C. Glitza, S.E. Woodman, I.I. Wistuba, R.N. Amaria, V. Prieto, R.E. Davis, W.W. Overwijk, A.H. Sharpe, J. Hu, P.A. Futreal, J. Blando, P. Sharma, J.P. Allison, L. Chin, J.A. Wargo

Administrative, technical, or material support (i.e., reporting or organizing data, constructing databases): P.-L. Chen, Z.A. Cooper, C.N. Spencer, P.A. Prieto, V. Gopalakrishnan, H. Jiang, R.J. Broaddus, L. Haydu, J.P. Allison, L. Chin, J.A. Wargo

Study supervision: P.-L. Chen, Z.A. Cooper, C.N. Spencer, R.J. Broaddus, J.P. Allison, L. Chin, J.A. Wargo

Grant Support

J.A. Wargo acknowledges the Melanoma Research Alliance Team Science Award, the Kenedy Memorial Foundation grant #0727030, U54CA163125, a STARS award, UT Regents, and the generous philanthropic support of several families whose lives have been affected by melanoma. This work was supported by NIH grants 1K08CA160692-01A1 (J.A. Wargo), U54CA163125 (Z.A. Cooper, J.A. Wargo, and L. Chin), T32CA009599 (P.A. Prieto), T32CA163185 (P.-L. Chen and W.-S. Chen), and 2P30CA016672 (I.I. Wistuba). W. Roh is supported by the CPRIT Graduate Scholar Award. I.C. Glitza holds a Conquer Cancer Foundation ASCO Young Investigator Award. L. Chin is a CPRIT Scholar in Cancer Research and was supported by a grant from the Cancer Prevention Research Institute of Texas (R1204). P.A. Futreal holds CPRIT funding (R1205 01), a Robert Welch Distinguished University Chair (G-0040), and a STARS award. R.N. Amaria has received research support from Merck, Novartis/Array, and Bristol-Myers Squibb. W.-J. Hwu has received research support from Bristol-Myers Squibb, Merck, GlaxoSmithKline, and MedImmune. I.I. Wistuba has received support from MD Anderson's Institutional Tissue Bank. This work was supported by MD Anderson's Institutional Tissue Bank Award (2P30CA016672) from the National Cancer Institute. This study was also supported by philanthropic contributions to The University of Texas MD Anderson Cancer Center Melanoma Moon Shot Program.

The costs of publication of this article were defrayed in part by the payment of page charges. This article must therefore be hereby marked *advertisement* in accordance with 18 U.S.C. Section 1734 solely to indicate this fact.

Received December 31, 2015; revised June 7, 2016; accepted June 10, 2016; published OnlineFirst June 14, 2016.

REFERENCES

1. Hodi FS, O'Day SJ, McDermott DF, Weber RW, Sosman JA, Haanen JB, et al. Improved survival with ipilimumab in patients with metastatic melanoma. N Engl J Med 2010;363:711–23.

2. Topalian SL, Hodi FS, Brahmer JR, Gettinger SN, Smith DC, McDermott DF, et al. Safety, activity, and immune correlates of anti–PD-1 antibody in cancer. N Engl J Med 2012;366:2443–54.
3. Andtbacka RH, Kaufman HL, Collichio F, Amatruda T, Senzer N, Chesney J, et al. Talimogene laherparepvec improves durable response rate in patients with advanced melanoma. J Clin Oncol 2015;33:2780–8.
4. Larkin J, Chiarion-Sileni V, Gonzalez R, Grob JJ, Cowey CL, Lao CD, et al. Combined nivolumab and ipilimumab or monotherapy in untreated melanoma. N Engl J Med 2015;373:23–34.
5. Postow MA, Chesney J, Pavlick AC, Robert C, Grossmann K, McDermott D, et al. Nivolumab and ipilimumab versus ipilimumab in untreated melanoma. N Engl J Med 2015;372:2006–17.
6. Wolchok JD, Kluger H, Callahan MK, Postow MA, Rizvi NA, Lesokhin AM, et al. Nivolumab plus ipilimumab in advanced melanoma. N Engl J Med 2013;369:122–33.
7. Brahmer JR, Tykodi SS, Chow LQ, Hwu WJ, Topalian SL, Hwu P, et al. Safety and activity of anti–PD-L1 antibody in patients with advanced cancer. N Engl J Med 2012;366:2455–65.
8. Curti BD, Kovacsovics-Bankowski M, Morris N, Walker E, Chisholm L, Floyd K, et al. OX40 is a potent immune-stimulating target in late-stage cancer patients. Cancer Res 2013;73:7189–98.
9. Topalian SL, Sznol M, McDermott DF, Kluger HM, Carvajal RD, Sharfman WH, et al. Survival, durable tumor remission, and long-term safety in patients with advanced melanoma receiving nivolumab. J Clin Oncol 2014;32:1020–30.
10. Wolchok JD, Weber JS, Maio M, Neyns B, Harmankaya K, Chin K, et al. Four-year survival rates for patients with metastatic melanoma who received ipilimumab in phase II clinical trials. Ann Oncol 2013;24:2174–80.
11. Schadendorf D, Hodi FS, Robert C, Weber JS, Margolin K, Hamid O, et al. Pooled analysis of long-term survival data from phase II and Phase III trials of ipilimumab in unresectable or metastatic melanoma. J Clin Oncol 2015;33:1889–94.
12. Rizvi NA, Hellmann MD, Snyder A, Kvistborg P, Makarov V, Havel JJ, et al. Cancer immunology. Mutational landscape determines sensitivity to PD-1 blockade in non-small cell lung cancer. Science 2015;348:124–8.
13. Snyder A, Makarov V, Merghoub T, Yuan J, Zaretsky JM, Desrichard A, et al. Genetic basis for clinical response to CTLA-4 blockade in melanoma. N Engl J Med 2014;371:2189–99.
14. Tumeh PC, Harview CL, Yearley JH, Shintaku IP, Taylor EJ, Robert L, et al. PD-1 blockade induces responses by inhibiting adaptive immune resistance. Nature 2014;515:568–71.
15. Taube JM, Klein A, Brahmer JR, Xu H, Pan X, Kim JH, et al. Association of PD-1, PD-1 ligands, and other features of the tumor immune microenvironment with response to anti–PD-1 therapy. Clin Cancer Res 2014;20:5064–74.
16. Van Allen EM, Miao D, Schilling B, Shukla SA, Blank C, Zimmer L, et al. Genomic correlates of response to CTLA-4 blockade in metastatic melanoma. Science 2015;350:207–11.
17. Hugo W, Zaretsky JM, Sun L, Song C, Moreno BH, Hu-Lieskovan S, et al. Genomic and transcriptomic features of response to anti–PD-1 therapy in metastatic melanoma. Cell 2016;165:35–44.
18. Gubin MM, Zhang X, Schuster H, Caron E, Ward JP, Noguchi T, et al. Checkpoint blockade cancer immunotherapy targets tumour-specific mutant antigens. Nature 2014;515:577–81.
19. Das R, Verma R, Sznol M, Boddupalli CS, Gettinger SN, Kluger H, et al. Combination therapy with anti–CTLA-4 and anti–PD-1 leads to distinct immunologic changes in vivo. J Immunol 2015;194:950–9.
20. Koyama S, Akbay EA, Li YY, Herter-Sprie GS, Buczkowski KA, Richards WG, et al. Adaptive resistance to therapeutic PD-1 blockade is associated with upregulation of alternative immune checkpoints. Nat Commun 2016;7:10501.
21. Rooney MS, Shukla SA, Wu CJ, Getz G, Hacohen N. Molecular and genetic properties of tumors associated with local immune cytolytic activity. Cell 2015;160:48–61.
22. Spranger S, Bao R, Gajewski TF. Melanoma-intrinsic beta-catenin signalling prevents anti-tumour immunity. Nature 2015;523:231–5.
23. Huang RR, Jalil J, Economou JS, Chmielowski B, Koya RC, Mok S, et al. CTLA4 blockade induces frequent tumor infiltration by activated lymphocytes regardless of clinical responses in humans. Clin Cancer Res 2011;17:4101–9.
24. Ferrara N, Kerbel RS. Angiogenesis as a therapeutic target. Nature 2005;438:967–74.
25. Voron T, Colussi O, Marcheteau E, Pernot S, Nizard M, Pointet AL, et al. VEGF-A modulates expression of inhibitory checkpoints on CD8+ T cells in tumors. J Exp Med 2015;212:139–48.
26. Ott PA, Hodi FS, Buchbinder EI. Inhibition of immune checkpoints and vascular endothelial growth factor as combination therapy for metastatic melanoma: an overview of rationale, preclinical evidence, and initial clinical data. Front Oncol 2015;5:202.
27. Westin JR, Chu F, Zhang M, Fayad LE, Kwak LW, Fowler N, et al. Safety and activity of PD1 blockade by pidilizumab in combination with rituximab in patients with relapsed follicular lymphoma: a single group, open-label, phase 2 trial. Lancet Oncol 2014;15:69–77.
28. Motz GT, Santoro SP, Wang LP, Garrabrant T, Lastra RR, Hagemann IS, et al. Tumor endothelium FasL establishes a selective immune barrier promoting tolerance in tumors. Nat Med 2014;20:607–15.
29. Ohm JE, Gabrilovich DI, Sempowski GD, Kisseleva E, Parman KS, Nadaf S, et al. VEGF inhibits T-cell development and may contribute to tumor-induced immune suppression. Blood 2003;101:4878–86.
30. Gabrilovich D, Ishida T, Oyama T, Ran S, Kravtsov V, Nadaf S, et al. Vascular endothelial growth factor inhibits the development of dendritic cells and dramatically affects the differentiation of multiple hematopoietic lineages in vivo. Blood 1998;92:4150–66.
31. Terme M, Pernot S, Marcheteau E, Sandoval F, Benhamouda N, Colussi O, et al. VEGFA-VEGFR pathway blockade inhibits tumor-induced regulatory T-cell proliferation in colorectal cancer. Cancer Res 2013;73:539–49.
32. Hodi FS, Lawrence D, Lezcano C, Wu X, Zhou J, Sasada T, et al. Bevacizumab plus ipilimumab in patients with metastatic melanoma. Cancer Immunol Res 2014;2:632–42.
33. Yuan J, Zhou J, Dong Z, Tandon S, Kuk D, Panageas KS, et al. Pretreatment serum VEGF is associated with clinical response and overall survival in advanced melanoma patients treated with ipilimumab. Cancer Immunol Res 2014;2:127–32.
34. Kageshita T, Hirai S, Ono T, Hicklin DJ, Ferrone S. Down-regulation of HLA class I antigen-processing molecules in malignant melanoma: association with disease progression. Am J Pathol 1999;154:745–54.
35. Shukla SA, Rooney MS, Rajasagi M, Tiao G, Dixon PM, Lawrence MS, et al. Comprehensive analysis of cancer-associated somatic mutations in class I HLA genes. Nat Biotechnol 2015;33:1152–8.
36. Taube JM, Anders RA, Young GD, Xu H, Sharma R, McMiller TL, et al. Colocalization of inflammatory response with B7-h1 expression in human melanocytic lesions supports an adaptive resistance mechanism of immune escape. Sci Translat Med 2012;4:127ra37.
37. Waggott D, Chu K, Yin S, Wouters BG, Liu FF, Boutros PC. NanoStringNorm: an extensible R package for the pre-processing of NanoString mRNA and miRNA data. Bioinformatics 2012;28:1546–8.
38. Vandesompele J, De Preter K, Pattyn F, Poppe B, Van Roy N, De Paepe A, et al. Accurate normalization of real-time quantitative RT-PCR data by geometric averaging of multiple internal control genes. Genome Biol 2002;3:Research0034.
39. Benjamini Y, Hochberg Y. Controlling the false discovery rate: a practical and powerful approach to multiple testing. J Royal Stat Soc Series B (Methodological) 1995;57:289–300.
40. Pounds S, Morris SW. Estimating the occurrence of false positives and false negatives in microarray studies by approximating and partitioning the empirical distribution of p-values. Bioinformatics 2003;19:1236–42.
41. Bates D, Maechler M, Bolker B, Walker S. Fitting linear mixed-effects models using lme4. J Stat Software 2015;67:1–48.
42. O'Connor CM, Sheppard S, Hartline CA, Huls H, Johnson M, Palla SL, et al. Adoptive T-cell therapy improves treatment of canine non-Hodgkin lymphoma post chemotherapy. Sci Rep 2012;2:249.
43. Ma W, Yang D, Gu Y, Guo X, Zhao W, Guo Z. Finding disease-specific coordinated functions by multi-function genes: insight into the coordination mechanisms in diseases. Genomics 2009;94:94–100.